A multi-omic analysis of optineurin proteinopathy in a yeast model suggests the involvement of lipid metabolism in Amyotrophic Lateral Sclerosis

Daniel M. Bean[1, 2, 3], Silvia Hnatova[2], Michael Mülleder[3], Sandra Magalhães[4, 5], Daniel J. H. Nightingale[6], Kathryn S. Lilley[6], Markus Ralser[2,3], Alexandra Nunes[4,5], Brian J. Goodfellow[5], Stephen G. Oliver[2, 3]

1. King's College London, Department of Biostatistics and Health Informatics, Institute of Psychiatry, Psychology and Neuroscience, De Crespigny Park, London SE5 8AF, United Kingdom
2. Cambridge Systems Biology Centre, University of Cambridge, Cambridge CB2 1GA, United Kingdom
3. Department of Biochemistry, University of Cambridge, Cambridge CB2 1GA, United Kingdom
4. iBiMED & Department of Medical Sciences, Campus Universitário de Santiago, University of Aveiro, 3810-193 Aveiro, Portugal
5. CICECO & Department of Chemistry, Campus Universitário de Santiago, University of Aveiro, 3810-193 Aveiro, Portugal
6. Cambridge Centre for Proteomics, Department of Biochemistry, University of Cambridge, Cambridge CB2 1QR, United Kingdom

Corresponding author:
Brian J. Goodfellow
CICECO & Department of Chemistry, University of Aveiro, 3810-193 Aveiro, Portugal
Email: brian.goodfellow@ua.pt
Tel: +351 234 401 506

Abstract

Amyotrophic Lateral Sclerosis (ALS) is an incurable fatal neurodegenerative disease for which the precise mechanisms of toxicity remain unclear despite some significant advances in our understanding of the underlying genetic basis. A holistic, integrated view of cellular changes will be critical to understanding the processes of neurodegeneration and the development of effective treatments. Mutant forms of optineurin (a ubiquitin-binding protein involved in autophagy, membrane trafficking, and NF-κB activation) are found associated with cytoplasmic inclusions containing TDP43 or SOD1 in some ALS patients. We have taken a multi-omics approach to understand the cellular response to OPTN overexpression in a yeast model of ALS. We found that genetic interaction screens and metabolomics provided parallel, highly complementary data on OPTN toxicity. Genetic enhancers of OPTN toxicity in yeast relate directly to the native function of OPTN in vesicular trafficking and intracellular transport, suggesting the human OPTN protein is functional when expressed in yeast even though there is no yeast ortholog. Crucially, we find that the genetic modifiers and the metabolic response are distinct for different ALS-linked genes expressed in yeast. This lends strong support to the use of yeast as a model system and omics platform to study ALS.

Keywords

ALS; Systems Biology; Metabolomics

52 ## Introduction

53 Amyotrophic Lateral Sclerosis (ALS) is a fatal neurodegenerative disease for which
54 there is no effective treatment available. ALS has been divided into familial (FALS) and
55 sporadic (SALS) forms on the basis of family history, with FALS patients accounting
56 for 5% of all ALS cases overall, but this dichotomy is now questioned[1]. Despite our
57 incomplete picture of the genetic landscape of ALS, it is considered a genetic disease.
58 Associated genetic variants, particularly the hexanucleotide repeat expansion of
59 C9orf72[2,3] and mutations in SOD1[4], TDP43[5,6] and FUS[7,8], are the basis for
60 experimental models of ALS in most model systems. Genetic variants and model
61 organism studies implicate a wide range of cellular pathways in the neurodegenerative
62 processes occurring in ALS, including oxidative stress, RNA metabolism, protein
63 aggregation and degradation (autophagy, and the ubiquitin-proteasome system), and
64 intracellular trafficking[9]. The hallmark histopathological feature of ALS is the
65 presence of intracellular protein aggregates. In most cases, these aggregates contain the
66 TDP43 protein, even though mutations in the TDP43 gene are only a rare cause of ALS.
67 A notable exception is patients with SOD1 mutations, where intracellular aggregates
68 contain the SOD1 protein, but not TDP43. With such a complex pathology
69 underpinning ALS, it is vital to develop multi-omics approaches to understand how the
70 interaction of multiple pathways is driving disease progression.
71
72 The OPTN gene encodes Optineurin, a ubiquitin-binding protein involved in
73 autophagy[10–12] membrane trafficking[13] and NF-κB activation[14]. ALS-linked
74 OPTN mutations were first detected in a Japanese cohort of ALS patients[15], where
75 OPTN protein was also found colocalized in cytoplasmic inclusions containing TDP43
76 or SOD1, suggesting OPTN is broadly involved in ALS regardless of the underlying

77 mutation. Subsequent studies indicated that that OPTN mutations are relatively more
78 common in Asian populations[15–19], and more rare in Caucasian ALS patients[20–
79 23]. Mutations in OPTN are also linked to primary open-angle glaucoma[24] and
80 Paget's disease of bone[25–27], suggesting that OPTN itself is a key driver of toxicity.
81 Compared to other ALS-linked proteins, there is relatively little research focused on
82 OPTN-ALS. We therefore chose to focus our study on OPTN specifically. The
83 intracellular pathways in which OPTN is involved are strongly conserved between yeast
84 and human cells[28,29]; however, there is no yeast ortholog of optineurin.
85
86 Two previous studies have used a yeast model to study OPTN[30,31]. In the first such
87 study, Kryndushkin et al. found that both wild-type and mutant OPTN formed
88 intracellular aggregates and were toxic to yeast[31]. More recently, Jo et al. performed a
89 screen for yeast single-gene deletions that modify the toxicity of human OPTN in
90 yeast[30]. Their screen used a high-copy plasmid to express OPTN, resulting in a level
91 of toxicity that is too high to reliably detect enhancer phenotypes (as the authors also
92 note). Our study builds on this previous work in two main ways. First, we expressed the
93 OPTN coding sequence from a low copy-number CEN plasmid, to get lower toxicity
94 levels and enable the detection of both suppressors and enhancers. Secondly, we also
95 carried out a metabolomic screen to build up a more detailed multi-omic picture of
96 OPTN-ALS.
97

98 ## Results

99 **Expression of wild-type human OPTN is toxic in yeast**

100 In line with similar studies[30–35], we cloned human OPTN into yeast expression
101 vectors under the control of the GAL promoter to allow rapidly-inducible strong

102 expression of the transgene. We first confirmed previous results which showed OPTN
103 expression is toxic and that the protein forms aggregates when expressed in
104 yeast[30,31]. Spot tests and liquid culture growth assays both demonstrated the reduced
105 growth of cells expressing OPTN-YFP vs YFP controls (Figure 1). Microscopy
106 demonstrated that OPTN-YFP formed intracellular aggregates in yeast, whereas YFP
107 alone remained diffuse in the cytoplasm (Figure 1). As found previously[31], OPTN
108 tended to aggregate as a single point, whereas TDP-43 and FUS formed multiple diffuse
109 aggregates (not shown).
110
111 Although there appeared to be a growth phenotype for the E478G mutant in the spot
112 test, this was not confirmed in the liquid culture. Furthermore, the fluorescence of the
113 YFP tag was not detectable for OPTN-E478G-YFP under the same microscopy
114 conditions or in a Western blot. We therefore used only the wild-type OPTN construct
115 for all experiments in this study.
116
117 **Genetic screening identifies protective genes**
118 Genetic modifiers of OPTN toxicity were identified using high-throughput synthetic
119 genetic array (SGA) screens[36] to introduce the OPTN-YFP or control plasmids into
120 the BY4741 deletion library. Screens were carried out in biological triplicate, each of
121 which also contained 4 technical repeats. Hits from the screen were defined as strains
122 whose interaction score was greater than 2 standard deviations away from the mean
123 interaction score in all 3 biological repeats, with at least 3 of 4 technical repeats scored
124 and normal growth on SGlu.
125

126 We identified 30 suppressors and 64 enhancers of the OPTN growth phenotype
127 (Supplementary Table S1). The only enriched GO term for the suppressors of OPTN
128 toxicity was cytoplasmic translation, suggesting that these genes are not specific
129 suppressors of OPTN but instead affect the expression of OPTN from the plasmid. We
130 therefore focused on the enhancers of OPTN toxicity. Deletion of these enhancer genes
131 increases OPTN toxicity, which suggests their protein products exert a protective effect
132 when present.
133
134 The enriched GO terms for the enhancers are shown in Table 1. The most enriched
135 process was "mitochondrion-ER membrane tethering", which is known to be a key
136 regulator of cell death processes[37]. Several of the enriched terms relate to intracellular
137 trafficking, specifically ER-to-Golgi, which is striking as OPTN plays a major role in
138 Golgi transport and membrane trafficking processes in human cells. Of the 64
139 suppressors, 52 have at least one human ortholog. The human orthologs are also
140 enriched for vesicle-mediated transport pathways, including ER-to-Golgi transport and
141 Golgi vesicle transport, which suggests the screen results could be translatable to human
142 cells.
143 Jo et al. recently performed a related OPTN screen in which human OPTN was
144 expressed from a high copy plasmid and genetic interactions were measured using
145 pooled barcode sequencing[30]. Their detected 127 suppressors of toxicity they
146 identified, none is significant as a suppressor or enhancer in our screen (enhancers were
147 unreliable). However, several of the same pathways were implicated by the hits in both
148 studies, particularly lipid metabolism and vesicle-mediated transport.
149

150 **Network analysis of protective genes**

151 Given the coherent set of enriched GO terms for these genes, we expected that they, or
152 their products, were likely to genetically or physically interact. Indeed 52/64 of the
153 protective genes interact genetically, and 41/64 of their protein products interact
154 physically (Figure S1). The genetic interaction network is a single component with 232
155 edges, whereas there are 4 separate components in the protein-protein interaction (PPI)
156 network (containing 32, 4, 3 and 2 proteins, respectively). Together, the genetic and
157 protein interactions connect 55/64 protective genes as a single component with 279
158 edges. The Syntaxin-like t-SNARE, TLG2 has high centrality (degree, betweeness, and
159 closeness) in both the genetic and protein interaction networks. TLG2 is the yeast
160 ortholog of mammalian Syntaxin-16, which functions in the ER-Golgi vesicle-mediated
161 transport pathway. It is possible that deletion of TLG2 enhances the toxicity of OPTN in
162 yeast by impairing trafficking to the vacuole, thus limiting protein degradation via this
163 pathway. However, previous work in HEK cells found the ubiquitin-proteasome system
164 to be the primary pathway responsible for degradation of OPTN[38].

165

166 **Genetic modifiers of OPTN toxicity have little overlap with TDP43 or FUS**
167 **modifiers in yeast**

168 To determine whether the hits from our screen are specific to OPTN or simply represent
169 a generic response to the expression of a toxic transgene, we compared our results to
170 those of previous SGA screens for TDP43[35] (8 suppressors, 6 enhancers)and FUS[33]
171 (36 suppressors, 24 enhancers) in yeast. These genetic modifiers have limited overlap,
172 consistent with the relevance of our hits to the endogenous function of OPTN. All genes
173 identified as modifiers in more than one screen are shown in Table 2.

174

175 The only overlapping genetic modifiers for OPTN were with FUS, with 3 common
176 enhancers and 2 common suppressors. Deletion of the MAP kinase gene SLT2
177 enhanced the toxic phenotype of both OPTN and FUS, potentially due to dysregulation
178 of peroxisome assembly or the unfolded protein response, both of which are regulated
179 by Slt2p. In a recent study, Jo et al. found that pharmacological inhibition of MAP2K5,
180 an upstream regulator of MAPK7, is a potential target for ALS therapy[30]. The 2 other
181 common enhancers, KGD2 and COX5A, encode mitochondrial proteins involved in the
182 TCA cycle (KGD2) and the inner mitochondrial membrane electron transport chain
183 (COX5A). Both deletions cause a severe reduction in growth rate and may be false
184 positives as the additional effect of OPTN is small.
185
186 Two suppressor deletions (rpl19b and rpp2b) were common to the OPTN and FUS
187 screens. Both genes encode ribosomal proteins and therefore affect cytoplasmic
188 translation. It is therefore possible that the protective phenotype is due to lowered
189 expression of the toxic transgene rather than a specific interaction. Finally, despite their
190 more similar cellular functions, only MRPL39, was identified (as an enhancer) in both
191 the TDP43 and FUS screens.
192
193 **MS and NMR identification of altered metabolites and lipids**
194 Given that the genetic modifiers of OPTN toxicity were distinct from those previously
195 identified for the ALS risk genes FUS and TDP43, we wondered whether strains
196 expressing these human proteins are also metabolically distinct. The stationary phase
197 (72hr) endometabolomes of yeast strains overexpressing OPTN, FUS and TDP43 were
198 therefore compared to controls using untargeted metabolic profiling by NMR and
199 targeted profiling by MS. A PCA analysis of OD- and TSP-normalized and pareto-

200 scaled NMR data matrices indicated that the profiles are, in fact, distinct
201 (Supplementary Figure S2A) and thus the metabolic differences are due to the specific
202 overexpressed protein. The targeted MS analysis of both the aqueous and lipid fractions
203 (Supplementary Figure S2B) from the same samples confirmed this.
204 The statistically significant metabolites (from MS and NMR data) that were altered in
205 OPTN samples compared to controls were identified and the effect size calculated
206 (Figure 2).
207 Metabolites whose levels increase when OPTN is overexpressed include those
208 associated with cellular and metabolic stress - such as γ-aminobutyric acid (GABA),
209 oxidized glutathione, glycerol, and trehalose. Many others are related to cellular energy
210 processes such as the TCA cycle, glycolysis and gluconeogenesis
211 (phosphoenolpyruvate, glutamine; Gln, glutamic acid, adenine nucleotides, and malate).
212 The most significantly increased metabolite was orotidylic acid followed by uridine-
213 diphosphate-N-acetylglucosamine (UDP-GlcNAc) and glycerol, while the metabolites
214 that decreased include the basic amino acids leucine and isoleucine; the TCA cycle
215 intermediates, succinate and citrate; and glycerophosphocholine (GPC).
216
217 Metaboanalyst 4.0[39] was used to identify the pathways most affected by the presence
218 of overexpressed OPTN compared to controls (Figure 3). The pathways affected that
219 have the highest impact include: alanine, aspartate and glutamate metabolism; glycine,
220 serine and threonine metabolism; arginine and proline metabolism and glutathione
221 metabolism. Pathways with high significance but lower impact include: butanoate
222 metabolism; pyrimidine/purine metabolism and glycerolipid metabolism.
223

224 To confirm the effect of OPTN on lipid metabolism indicated in the Metaboanalyst
225 results, we also profiled the endometabolome using LC-MS on the organic phase
226 extract. Distinct profiles were again observed (Figure S2B) for OPTN, FUS and TDP43
227 and 75 (37 negative ion + 38 positive ion) statistically significant m/z species were
228 identified as increased in cells overexpressing OPTN, while 78 (28 negative ion + 50
229 positive ion) species decreased. Of these, a reduced group was selected based on an
230 effect size above or below 4 and with VIPs larger than 1.56 from a UV-scaled PLS-DA
231 model using the positive ion mode data and ES above or below 4 and VIPS above 1.68
232 for the negative ion mode data. Identified lipid families are shown in Table 3 and the
233 associated m/z ions and tentative identification in Supplementary Table S2.
234

235 **Discussion**

236 In this study, we have generated genome-wide genetic interaction data and carried out a
237 metabolomic screen on the same OPTN yeast model. Significantly, we show that in
238 both profiles, yeast cells expressing OPTN are distinct from yeast cells expressing other
239 human genes associated with ALS (TDP-43 and FUS). We have also identified genetic
240 modifiers of OPTN toxicity that are directly related to the endogenous function of
241 OPTN in human cells.
242

243 The wild-type OPTN protein was toxic when expressed in yeast, consistent with related
244 studies of other ALS genes[30,31,33–35,40]. The ALS-linked OPTN mutant E478G
245 was not efficiently expressed in our system, and therefore we used the wild-type protein
246 for all screens. Although we are therefore unable to model the effect of the specific
247 mutations linked to ALS, a significant part of ALS pathology appears to be a
248 proteinopathy, which is recapitulated in this system. For example, Armakola et al. used

249 wild-type TDP-43 for a genome-wide yeast screen and identified dbr1 as a modifier
250 gene that was validated in human neuronal cell lines[35]. Therefore, whilst this system
251 models only part of the pathology of ALS, previous data suggest that results in this type
252 of system are translatable to human cells.
253
254 Crucially, the growth phenotype of this yeast proteinopathy model is not a generic
255 response to an overexpressed transgene, as might have been expected. This is shown by
256 the distinct modifiers identified for the ALS-linked genes FUS, TDP-43 and OPTN in
257 genetic interaction screens and in our metabolic profiling. One possible mechanism for
258 these distinct modifiers is that the expressed proteins retain at least part of their
259 endogenous function when expressed in yeast. Yeast is widely used for recombinant
260 protein production, both for research and commercial applications. Whilst the correct
261 folding of any particular recombinant protein is not guaranteed, and a substrate (and/or
262 cofactor) required to carry out that protein's molecular function may not be available in
263 yeast, it is possible that the OPTN protein retains its native molecular function when
264 expressed in yeast.
265
266 In a seminal work, Kachroo et al.[41] found that almost half of the deletion of 414
267 essential yeast genes could be complemented ("humanised") by the expression of their
268 human ortholog. Although yeast does not possess an OPTN ortholog, the function of
269 this human protein may be retained through interaction with conserved components of
270 the same pathways. For example, yeast also does not have any orthologs of the Bcl-2
271 apoptosis regulator proteins, yet expression of mammalian Bax protein induces cell
272 death[42,43], apparently though a mechanism conserved in human cells[44]. Taken
273 together with the direct relevance of the modifiers we identify in our genetic screen to

274 the endogenous function of OPTN (specifically intracellular trafficking and ER-Golgi
275 transport), and the differing metabolic profiles of FUS, TDP-43 and OPTN, we suggest
276 that the phenotype of yeast expressing transgenic OPTN is due to the native properties
277 or functions of the OPTN protein, and not simply due to its overexpression.
278
279 The metabolic profiling results suggest that OPTN is affecting the TCA cycle, which
280 may be related to general mitochondrial dysfunction. As overexpression of a non-native
281 protein in yeast would also be expected to induce the UPR (and ER stress), the
282 increased levels of some amino acids may be a result of this process causing increased
283 protein catabolism, a reduction in protein biosynthesis or a reduction in amino acid
284 utilization/biosynthesis. Oxidative stress was increased in OPTN yeast compared to
285 controls as the GSH_{red}/GSH_{ox} ratio is 1.4 times lower in these cells (Supplementary
286 Figure S3). Interestingly, an increase in the amino acid proline is seen in OPTN
287 expressing yeast. As the presence of this amino acid has been found to minimize protein
288 aggregation and the depletion of proline has been linked to the inhibition of the
289 UPR[45], our results are consistent with OPTN aggregation and triggering of the UPR
290 in our yeast system. Increased UDP-GlcNAc levels suggests that cell wall biosynthesis
291 may be decreased, and lipid metabolism also appears to be altered as indicated by a
292 decrease in GPC and an increase in Ser and in UDP-glucose, both involved in
293 sphingolipid biosynthesis. As UDP-GlcNAc is also intimately involved in the
294 production of N-glycans, with biosynthesis first taking place in the ER and subsequently
295 in the Golgi apparatus, any disruption in trafficking between these organelles could also
296 affect UDP-GlcNAc levels. This may corroborate our conclusion that the phenotype of
297 yeast cell expressing OPTN reflects the native function of the protein (ER-Golgi
298 transport) and is not a generic response to an exogenous protein. Our profiling data also

299 indicates that orotidylic acid had the largest increase of all the aqueous assigned
300 metabolites detected in our study. At this time, we do not have an explanation as to the
301 significance of this perturbation.
302
303 A number of metabolomic biomarkers have been proposed for neurological diseases
304 including ALS[46–49]. The results from Wuolikainen et al.[46] show some correlation
305 with our results where 3 of the top 5 positively correlated ALS metabolites (Pro, Trp,
306 AMP) in plasma are also seen as increased in our OPTN cells. A deficit in RNA
307 synthesis was also seen, suggesting a decrease in the PPP. The decrease in ribose-5-
308 phosphate seen in our yeast model is consistent with this. Basic amino acids were also
309 indicated as potential biomarkers in CSF and plasma. However, we see decreases in
310 yeast, while increases are seen in human fluids. A recent metabolomic study of a
311 neuronal cellular model of ALS[50] included analysis of metabolite variations seen for
312 cells overexpressing SOD1 and G93A SOD1 under serum deprivation. These results, in
313 general, compare well with those found in our OPTN stationary-phase yeast model.
314
315 Our lipid data from LC-MS profiling indicated that many lipid species were
316 significantly increased in OPTN-expressing cells (16 increasing above ES 7 compared
317 to 2 decreasing). In fact, only OPTN (and not FUS or TDP43) showed a larger number
318 of increased lipids compared to decreased lipids. Thus, OPTN appears to affect lipid
319 metabolism even as an exogenous protein in yeast. An LC-MS profiling study of the
320 lipidome for the CSF of ALS patients has identified a number of lipid biomarkers for
321 ALS[46]. Phosphatidylcholines, sphingomyelins, glucosylceramides and sterols were
322 found to be increased, while TAG was decreased in ALS patients. We also see increases
323 in lipids from these families in OPTN-overexpressing yeast cells. Although in a

324 different model, two ALS studies using different SOD1 mutated mice[51,52] also
325 demonstrated that lipids such as sphingolipids, ceramides and glucosylceramides are
326 increased in spinal cord fluid and skeletal muscle. Therefore, it appears that OPTN may
327 be producing a yeast phenotype that reflects lipidome effects seen in in vivo situations.
328
329 We have studied genetic interactions, integrating those results with protein interaction
330 data, and metabolites. However, additional 'omics approaches could, and should, be
331 added to build both a broad and deep intracellular understanding of ALS. This
332 panoramic view of ALS is necessary to predict the impact of perturbations to this
333 system either by mutation or, eventually, by treatment.
334

335 ## Methods

336 **Yeast strains and media**

337 The Synthetic Genetic Array (SGA)[36] starter strain Y7092 (MATα can1Δ::STE2pr-
338 Sp_his5 lyp1Δ his3Δ1 leu2Δ0 ura3Δ0 met15Δ0) was used for all experiments was
339 mated with the BY4741 deletion library in the SGA. Strains were manipulated, and
340 media prepared using standard microbiological techniques. Yeast were cultured in
341 synthetic minimal media without uracil, and with either 2% glucose (SGlu), 2%
342 raffinose (SRaf) or 2% galactose (SGal) as the carbon source.
343
344 To induce expression from the plasmid in liquid culture, single colonies were picked
345 into 50µl SGlu in a 96-well plate and incubated at 30˚C with shaking. After 24h, 10µl
346 of the SGlu cultures was inoculated into 200µl SRaf and incubated at 30˚C with
347 shaking. After 24h, 20µl of the SRaf cultures were inoculated into 100µl fresh SRaf and

348 incubated at 30˚C with shaking. SGal medium was inoculated with a 1:20 dilution of
349 this SRaf culture in either 96-well or 384-well plates.
350
351 For induction in the SGA, deletion mutants containing the plasmid were pinned onto
352 SGal plates at 384 colonies per plate. After incubation at 30˚C for 24h, these colonies
353 were pinned onto SRaf at 384 colonies per plate and incubated at 30˚C for 24h. Each
354 colony from the SRaf plates was pinned onto SGal 4 times (1536 colonies per plate),
355 and incubated at 30˚C. Plates were scanned at 300dpi after 48h of growth. All pinning
356 steps were performed using a Singer ROTOR HDA.
357
358 **Plasmid construction**
359 OPTN in pEGFP-C3 was kindly donated by Dr. Justin Yerbury. The OPTN ORF was
360 PCR amplified from pEGFP-C3 and cloned into the Gateway donor plasmid
361 pDONR221 (KanR) via the Gateway BP reaction according to the manufacturer's
362 instructions. The E478G mutation was introduced by site-directed mutagenesis using
363 the Aglient QuikChange II Site-Directed Mutagenesis Kit. Donor plasmids containing
364 FUS and TDP43 were kindly donated by the Gitler lab.
365
366 All pDONR221 Gateway donors were cloned into the Gateway destination vector
367 pAG416GAL-ccdb-EYFP[53] (CEN, URA3, AmpR, referred to as pAG416) obtained
368 from Addgene via the LR reaction, according to manufacturer instructions.
369
370 The empty pAG416 vector was modified to create the control (YFP only) plasmid by
371 removing the sequence between the GAL1 promoter and YFP. In the unmodified
372 pAG416, YFP is approximately 1750 bp from the GAL1 promoter, resulting in weak

373 expression. The YFP coding sequence was PCR-amplified from pAG416 and, in
374 parallel, pAG416 was digested with Kpn1 and Not1. The larger restriction fragment was
375 gel-purified and recombined with the PCR product in yeast. The resulting plasmid,
376 pAG416-short, was used as the control in all experiments.
377
378 All plasmid sequences were confirmed by restriction mapping and DNA sequencing.
379 YFP expression (either alone or as a tag) was confirmed by fluorescence microscopy
380 and Western blot using anti-GFP (AbCam antibody ab6556) and anti-histone H3
381 (AbCam ab1791) as a loading control. The presence of the expressed protein (OPTN,
382 TDP43 or FUS) was confirmed by in-gel digestion, followed by LC-MS/MS. Briefly,
383 yeast protein extraction for both western blotting and LC-MS/MS was performed
384 according to[54]. Total extract, corresponding to approximately 1.7 x 10^6 cells, was
385 resolved by SDS-PAGE gel electrophoresis. Following Coomassie staining, a band was
386 excised from the gel that corresponded to a ca. 20 kDa range around the predicted
387 molecular weight of the eYFP-tagged human protein. The band was dissected into cubes
388 of approximately 1 mm and destained (using ammonium bicarbonate), reduced (with
389 dithiothreitol) and alkylated (using iodoacetamide). The sample was digested for 16 h at
390 37C using a 1:50 (w/w) ratio of Sequencing Grade Modified Trypsin (Promega):protein
391 in the gel. The digest was analysed by LC-MS/MS on a nanoAcquity UPLC system
392 (Waters) coupled in-line to a LTQ Orbitrap Velos mass spectrometer (ThermoFisher
393 Scientific), essentially according to[55], but with the modification that MS2 scans were
394 performed on the twenty most intense ions per survey scan with a charge of 2+ or
395 above. In all cases, the human protein corresponding to the expressed transgene was
396 correctly identified in the LC-MS/MS data.
397

398 **Mass spectrometry data processing**

399 Raw mass spectrometry data files were converted to MGF format using MSConvert
400 (version 3.0.9283, Proteowizard). MGF files were searched using an in-house Mascot
401 server (version 2.6.0, Matrix Science) against three databases at the same time, which
402 were a canonical S. cerevisiae database, downloaded from UniProt (March 2017; 6,749
403 sequences), a canonical isoformal version of the human SwissProt database (November
404 2016; 42,144 sequences) and the cRAPome database of common mass spectrometry
405 contaminants[56] (January 2017; 115 sequences). Precursor tolerance was set to 20 ppm
406 and fragment tolerance to 0.6 Da. Carbamidomethylation of cysteine was specified as a
407 fixed modification and oxidation of methionine as a variable modification.

408

409 **Genetic interaction screen**

410 Genetic interactions were screened using Synthetic Genetic Array technology as
411 described[36], the only modification being the use of URA3 as the selectable marker for
412 the query strain (Y7092 transformed with OPTN-YFP or control plasmid) instead of
413 NatMX4. Interactions were scored from images scanned at 300dpi after 48h of growth
414 on SGal using Gitter[57] in SGAtools[58] (available at
415 http://sgatools.ccbr.utoronto.ca/). Colonies that failed to grow on SGlu media were
416 excluded from the analysis. Hits from the screen were defined as strains greater than 2
417 standard deviations away from the mean interaction score in all 3 biological repeats
418 with at least 3 of 4 technical repeats scored and normal growth on SGlu.

419

420 **Interaction networks**

421 Yeast interaction data was retrieved from the 06/11/2017 update of YeastMine[59]
422 (https://yeastmine.yeastgenome.org) and analysed in Cytoscape[60].

423

424 **Quenching and extraction of the endometabolome**

425 For all samples (TDP, FUS, OPTN) and controls two biological replicates were
426 prepared and two technical replicates used. After the final incubation in 25 ml galactose
427 medium (OD600 = 0.05) the samples were harvested at 72 hr and immediately placed
428 on ice. A protocol similar to Palomino-Schätzlein et al. (2013) was followed[61].
429 Pelleting and resuspension in cold phosphate buffer was carried out followed by
430 centrifugation and flash freezing in liquid nitrogen. For metabolite extraction, 500 µL of
431 methanol/chloroform (2:1) at 4°C was added to the frozen samples and the pellet was
432 resuspended by vortexing after 5 min. Five freeze/thaw cycles of 1 min in liquid
433 nitrogen and 2 min on ice were then carried out followed by addition of 250 µL of
434 chloroform and 250 µL of MilliQ water. Vortexing for 1 min was followed by a 30 min
435 centrifugation (20ºC, 16000 x g). The upper aqueous layer was collected carefully with
436 a Gilson pipette. The lipophilic phase was collected into a glass vial. The samples were
437 dried using a stream of N_2 gas (NitroFlowLab) on a Techne Dri-Block(R) DB30
438 (aqueous 2-4 hr, lipid 10 min). The aqueous samples were further dried in a speedvac
439 (1-2 hr, Savant Speed Vac(R) SPD111V). All extracts were stored at 4°C.

440

441 **NMR spectroscopy**

442 For the NMR analysis, the aqueous extracts were re-suspended in 620 µl D_2O, 0.01%
443 TSP and 100 mM pH 7.0 phosphate buffer (Na_2HPO_4 100 mM, pH 7.0). All samples
444 were centrifuged (1 min, 20 °C, 16,000 g) before transferring to 5mm NMR tubes. The
445 ^{1}H-NMR spectra were recorded at 298K on a Bruker Avance III 500 MHz spectrometer
446 using a TXI or TCI probe. 1D ^{1}H spectra were acquired using a NOESY pulse sequence
447 to suppress the water resonance, with a sweep width of 7002 Hz (14 ppm), 32k data

448 points, a recycle delay of 12 s, a mixing time of 100 ms and 128 scans per free
449 induction decay (FID).
450
451 **Mass spectrometry**
452 ***Aqueous fractions***
453 Metabolite concentrations for the aqueous fractions were determined on a liquid
454 chromatography (Agilent 1290 Infinity) and tandem mass spectrometry (Agilent 6460)
455 system. All compounds were identified by comparing retention time and fragmentation
456 pattern with analytical standards. The instrument was operated in single reaction
457 monitoring mode. Ion transitions and analytical methods used for metabolite
458 identification and concentration determination are given in Supplementary Tables S3
459 and S4. Metabolite concentrations were determined by external calibration. Solvents
460 were of UPLC grade and chemicals of at least analytical grade. Specific conditions for
461 amino acids, other polar metabolites and UDP-N-acetylglucosamine are given in
462 supplementary methods.
463
464 ***Lipid fractions***
465 Samples, re-suspended in 200µl of HPLC grade methanol, were analysed in both
466 positive and negative ion modes using a Waters Xevo G2 quadrupole time of flight (Q-
467 ToF) combined with an Acquity Ultra Performance Liquid Chromatogram (UPLC)
468 (Waters Corporation, Manchester, UK). Injection volumes and conditions along with
469 gradient parameters and data acquisition are given in supplementary methods.
470

Multivariate analysis

iNMR software (http://www.inmr.net) was used to process the NMR spectra with zero filling to 64k data points and 0.3 Hz line broadening being applied before Fourier transformation. The spectra were manually phased, baseline corrected, referenced to TSP at 0.00ppm and exported (0.5-9.5 ppm for aqueous phase, 0.5-8 ppm for lipid phase) as a matrix. The spectra were normalized to OD600 at the time of extraction and then to TSP. The OD600 values at the time of extraction were (mean ± standard deviation): control = 7.98 ± 0.14, TDP43 = 6.80 ± 0.09, FUS = 7.91 ± 0.08 and OPTN = 7.87 ± 0.15. The normalised spectra were then checked in iNMR and, if necessary, alignment was carried out using using the 'speaq' package in R. The water region was excluded from the alignment.

MVA were performed using the ropls package[62] in R. Initial Principal Components Analysis identified outliers that were excluded from subsequent analyses. The identification of metabolites for NMR was carried out by comparing the spectra with those of standard compounds from the Biological Magnetic Resonance Data Bank, the Yeast Metabolome Database and the Human Metabolome Database. The relative amounts of the NMR metabolites and the effect size were determined by integrating the area under the most well-separated metabolite peak in iNMR and then using in-house R scripts. MS metabolite concentrations were used directly after normalisation to OD600. Pairwise t-tests were carried out using the False Discovery Rate (FDR) to adjust for multiple testing. Effect sizes were calculated and corrected for small sample sizes using the formula:

$$Effect\ Size = (1 - (3/(4n1+n2-2) - 1))((x1-x2)/pooledSD)$$

495 where pooled SD is the pooled standard deviation, x1 and x2 are the mean levels of
496 metabolite x and n1 and n2 are the number of replicates. Metaboanalyst 4.0[39] was
497 used to identify enriched metabolic pathways. The final list of metabolites used
498 included 51 from the targeted MS analysis and 7 (orotidylic acid,
499 glycerophosphocholine, trehalose, glycerol, betaine, uracil and acetate) non-duplicated
500 metabolites from NMR.
501
502 For the lipid LCMS data, positive and negative ion mode deisotoped results were
503 normalised to total area and analysed as for aqueous NMR and MS data. Tentative
504 identification of lipids with statistically significant effect size differences was carried
505 out using m/z data and the LIPID MAPS Online Tools[63] (Supplementary Table S2).
506
507 **Data availability**
508 The metabolomics data has been deposited at Metabolights with access code,
509 MTBLS796.
510

511 ## Acknowledgements

512 The work of D.M.B., G.F., S.H. and S.G.O. was supported by the Wellcome
513 Trust/MRC (grant code: 089703/Z/09/Z). D.J.H.N. was supported by a BBSRC
514 Strategic Longer and Larger grant, awarded to K.S.L. (award BB/L002817/1)
515 The authors are grateful to Dr. Justin Yerbury for the OPTN plasmid, Prof. Aaron Gitler
516 for the TDP-43 and FUS plasmids and Dr. Mike Deery for LC-MS/MS analysis of our
517 plasmid overexpression samples. We thank Steven Murfitt (University of Cambridge)
518 for the acquisition of the LCMS/MS data for the endometabolome lipid fraction
519 samples.

B.J.G. and A.N. were supported by grants UID/BIM/04501/2013 and UID/CTM/50011/2013, co-funded by Fundação para a Ciência e Tecnologia I.P. (PIDDAC) and by European Regional Development Fund (FEDER) and POCI-01-0145-FEDER-007628 and POCI-01-0145-FEDER-007679, funded by the Operational Programme Competitiveness and Internationalization COMPETE 2020. S.M. is supported by Fundação para a Ciência e Tecnologia I.P. through the individual PhD grant SFRH/BD/131820/2017. The NMR spectrometers used in this work are part of the National NMR Network (PTNMR) and are partially supported by Infrastructure Project Nº 022161 (co-financed by FEDER through COMPETE 2020, POCI and PORL and FCT through PIDDAC).

This paper represents independent research part funded by the National Institute for Health Research (NIHR) Biomedical Research Centre at South London and Maudsley NHS Foundation Trust and King's College London. The views expressed are those of the author(s) and not necessarily those of the NHS, the NIHR or the Department of Health.

Author contributions

Conceptualisation – DMB, BJG, SGO

Formal Analysis – DMB, BJG

Funding Acquisition – SGO, BJG

Investigation – DMB, MM, SM, SH, DJHN

Supervision – KSL, MR, AN, BJG, SGO

Writing – Original Draft Preparation – DMB, BJG

Writing – Review and Editing – SGO, DMB, BJG, MM, SM, SH, DJHN, KSL, AN

545 **Conflict of interest**

546 The authors declare that no conflicts of interest exist.

547

548

549 **References**

550 1. Chiò A *et al.* 2014 Genetic counselling in ALS: facts, uncertainties and clinical
551 suggestions. *J. Neurol. Neurosurg. & Psychiatry* **85**, 478 LP-485.

552 2. Renton AE *et al.* 2011 A hexanucleotide repeat expansion in C9ORF72 is the
553 cause of chromosome 9p21-linked ALS-FTD. *Neuron*
554 (doi:10.1016/j.neuron.2011.09.010)

555 3. DeJesus-Hernandez M *et al.* 2011 Expanded GGGGCC Hexanucleotide Repeat
556 in Noncoding Region of C9ORF72 Causes Chromosome 9p-Linked FTD and
557 ALS. *Neuron* (doi:10.1016/j.neuron.2011.09.011)

558 4. Halper RDRSTPDFDASPHADDGJORJPDHXRDKAM-YDCAGSMBRTR. *et*
559 *al.* 1993 Mutations in Cu/Zn superoxide dismutase gene are associated with
560 familial amyotrophic lateral sclerosis. *Nature* **362**, 59–62.
561 (doi:10.1038/362059a0)

562 5. Kabashi E *et al.* 2008 TARDBP mutations in individuals with sporadic and
563 familial amyotrophic lateral sclerosis. *Nat. Genet.* (doi:10.1038/ng.132)

564 6. Sreedharan J *et al.* 2008 TDP-43 mutations in familial and sporadic amyotrophic
565 lateral sclerosis. *Science* (doi:10.1126/science.1154584)

566 7. Kwiatkowski TJ *et al.* 2009 Mutations in the FUS/TLS gene on chromosome 16
567 cause familial amyotrophic lateral sclerosis. *Science (80-.).*
568 (doi:10.1126/science.1166066)

569 8. Vance C *et al.* 2009 Mutations in FUS, an RNA Processing Protein, Cause

570 Familial Amyotrophic Lateral Sclerosis Type 6. *Science (80-.).*
571 (doi:10.1126/science.1165942)
572 9. Hardiman O, Al-Chalabi A, Chio A, Corr EM, Logroscino G, Robberecht W,
573 Shaw PJ, Simmons Z, Van Den Berg LH. 2017 Amyotrophic lateral sclerosis.
574 *Nat. Rev. Dis. Prim.* **3**. (doi:10.1038/nrdp.2017.71)
575 10. Dikic I *et al.* 2011 Phosphorylation of the Autophagy Receptor Optineurin
576 Restricts Salmonella Growth. *Science (80-.).* **333**, 228–233.
577 (doi:10.1126/science.1205405)
578 11. Wong YC, Holzbaur ELF. 2014 Optineurin is an autophagy receptor for damaged
579 mitochondria in parkin-mediated mitophagy that is disrupted by an ALS-linked
580 mutation. *Proc. Natl. Acad. Sci.* **111**, E4439–E4448.
581 (doi:10.1073/pnas.1405752111)
582 12. Sirohi K, Swarup G. 2016 Defects in autophagy caused by glaucoma-associated
583 mutations in optineurin. *Exp. Eye Res.* **144**, 54–63.
584 (doi:10.1016/j.exer.2015.08.020)
585 13. Nagabhushana A, Chalasani ML, Jain N, Radha V, Rangaraj N, Balasubramanian
586 D, Swarup G. 2010 Regulation of endocytic trafficking of transferrin receptor by
587 optineurin and its impairment by a glaucoma-associated mutant. *BMC Cell Biol.*
588 **11**. (doi:10.1186/1471-2121-11-4)
589 14. Zhu G, Wu CJ, Zhao Y, Ashwell JD. 2007 Optineurin Negatively Regulates
590 TNFα- Induced NF-κB Activation by Competing with NEMO for Ubiquitinated
591 RIP. *Curr. Biol.* **17**, 1438–1443. (doi:10.1016/j.cub.2007.07.041)
592 15. Maruyama H *et al.* 2010 Mutations of optineurin in amyotrophic lateral sclerosis.
593 *Nature* **465**, 223–226. (doi:10.1038/nature08971)
594 16. Li C, Ji Y, Tang L, Zhang N, He J, Ye S, Liu X, Fan D. 2015 Optineurin

595 mutations in patients with sporadic amyotrophic lateral sclerosis in China.
596 *Amyotroph. Lateral Scler. Front. Degener.* **16**, 485–489.
597 (doi:10.3109/21678421.2015.1089909)
598 17. Iida A *et al.* 2012 Novel deletion mutations of OPTN in amyotrophic lateral
599 sclerosis in Japanese. *Neurobiol. Aging* **33**.
600 (doi:10.1016/j.neurobiolaging.2011.12.037)
601 18. Iida A, Hosono N, Sano M, Kamei T, Oshima S, Tokuda T, Kubo M, Nakamura
602 Y, Ikegawa S. 2012 Optineurin mutations in Japanese amyotrophic lateral
603 sclerosis. *J. Neurol. Neurosurg. Psychiatry*. **83**, 233–235.
604 (doi:10.1136/jnnp.2010.234963)
605 19. Naruse H *et al.* 2012 Mutational analysis of familial and sporadic amyotrophic
606 lateral sclerosis with OPTN mutations in Japanese population. *Amyotroph.*
607 *Lateral Scler.* **13**, 562–566. (doi:10.3109/17482968.2012.684213)
608 20. Millecamps S *et al.* 2011 Screening of OPTN in French familial amyotrophic
609 lateral sclerosis. *Neurobiol. Aging* **32**.
610 (doi:10.1016/j.neurobiolaging.2010.11.005)
611 21. Johnson L, Miller JW, Gkazi AS, Vance C, Topp SD, Newhouse SJ, Al-Chalabi
612 A, Smith BN, Shaw CE. 2012 Screening for OPTN mutations in a cohort of
613 British amyotrophic lateral sclerosis patients. *Neurobiol. Aging* **33**.
614 (doi:10.1016/j.neurobiolaging.2012.06.023)
615 22. Del Bo R *et al.* 2011 Novel optineurin mutations in patients with familial and
616 sporadic amyotrophic lateral sclerosis. *J. Neurol. Neurosurg. Psychiatry* **82**,
617 1239–1243. (doi:10.1136/jnnp.2011.242313)
618 23. Belzil V V., Daoud H, Desjarlais A, Bouchard JP, Dupré N, Camu W, Dion PA,
619 Rouleau GA. 2011 Analysis of OPTN as a causative gene for amyotrophic lateral

620 sclerosis. *Neurobiol. Aging* **32**. (doi:10.1016/j.neurobiolaging.2010.10.001)
621 24. Rezaie T *et al.* 2002 Adult-Onset Primary Open-Angle Glaucoma Caused by
622 Mutations in Optineurin — Supplemental Data. *Science* **295**, 1077–1079.
623 (doi:10.1126/science.1066901)
624 25. Albagha OME *et al.* 2010 Genome-wide association study identifies variants at
625 CSF1, OPTN and TNFRSF11A as genetic risk factors for Paget's disease of
626 bone. *Nat. Genet.* **42**, 520–524. (doi:10.1038/ng.562)
627 26. Michou L, Conceição N, Morissette J, Gagnon E, Miltenberger-Miltenyi G, Siris
628 ES, Brown JP, Cancela ML. 2012 Genetic association study of UCMA/GRP and
629 OPTN genes (PDB6 locus) with Paget's disease of bone. *Bone* **51**, 720–728.
630 (doi:https://doi.org/10.1016/j.bone.2012.06.028)
631 27. Silva IAL, Conceição N, Gagnon É, Caiado H, Brown JP, Gianfrancesco F,
632 Michou L, Cancela ML. 2018 Effect of genetic variants of OPTN in the
633 pathophysiology of Paget's disease of bone. *Biochim. Biophys. Acta - Mol. Basis*
634 *Dis.* **1864**, 143–151. (doi:https://doi.org/10.1016/j.bbadis.2017.10.008)
635 28. Bonifacino JS, Glick BS. 2018 The Mechanisms of Vesicle Budding and Fusion.
636 *Cell* **116**, 153–166. (doi:10.1016/S0092-8674(03)01079-1)
637 29. Finley D, Ulrich HD, Sommer T, Kaiser P. 2012 The ubiquitin-proteasome
638 system of Saccharomyces cerevisiae. *Genetics* **192**, 319–360.
639 (doi:10.1534/genetics.112.140467)
640 30. Jo M *et al.* 2017 Yeast genetic interaction screen of human genes associated with
641 amyotrophic lateral sclerosis: Identification of MAP2K5 kinase as a potential
642 drug target. *Genome Res.* **27**, 1487–1500. (doi:10.1101/gr.211649.116)
643 31. Kryndushkin D, Ihrke G, Piermartiri TC, Shewmaker F. 2012 A yeast model of
644 optineurin proteinopathy reveals a unique aggregation pattern associated with

645 cellular toxicity. *Mol. Microbiol.* **86**, 1531–1547. (doi:10.1111/mmi.12075)
646 32. Couthouis J *et al.* 2011 A yeast functional screen predicts new candidate ALS
647 disease genes. *Proc. Natl. Acad. Sci. U. S. A.* **108**, 20881–90.
648 (doi:10.1073/pnas.1109434108)
649 33. Sun Z, Diaz Z, Fang X, Hart MP, Chesi A, Shorter J, Gitler AD. 2011 Molecular
650 determinants and genetic modifiers of aggregation and toxicity for the als disease
651 protein fus/tls. *PLoS Biol.* **9**. (doi:10.1371/journal.pbio.1000614)
652 34. Ju S *et al.* 2011 A Yeast Model of FUS/TLS-Dependent Cytotoxicity. *PLoS Biol.*
653 **9**, e1001052. (doi:10.1371/journal.pbio.1001052)
654 35. Armakola M *et al.* 2012 Inhibition of RNA lariat debranching enzyme suppresses
655 TDP-43 toxicity in ALS disease models. *Nat. Genet.* **44**, 1302–1309.
656 (doi:10.1038/ng.2434)
657 36. Baryshnikova A, Costanzo M, Dixon S, Vizeacoumar FJ, Myers CL, Andrews B,
658 Boone C. 2010 Synthetic genetic array (SGA) analysis in Saccharomyces
659 cerevisiae and schizosaccharomyces pombe. *Methods Enzymol.* **470**, 145–179.
660 (doi:10.1016/S0076-6879(10)70007-0)
661 37. Grimm S. 2012 The ER-mitochondria interface: The social network of cell death.
662 *Biochim. Biophys. Acta - Mol. Cell Res.* **1823**, 327–334.
663 (doi:10.1016/j.bbamcr.2011.11.018)
664 38. Mao J, Xia Q, Liu C, Ying Z, Wang H, Wang G. 2017 A critical role of Hrd1 in
665 the regulation of optineurin degradation and aggresome formation. *Hum. Mol.*
666 *Genet.* **26**, 1877–1889. (doi:10.1093/hmg/ddx096)
667 39. Xia J, Sinelnikov I V., Han B, Wishart DS. 2015 MetaboAnalyst 3.0-making
668 metabolomics more meaningful. *Nucleic Acids Res.* **43**, W251–W257.
669 (doi:10.1093/nar/gkv380)

670 40. Johnson BS, McCaffery JM, Lindquist S, Gitler AD. 2008 A yeast TDP-43
671 proteinopathy model: Exploring the molecular determinants of TDP-43
672 aggregation and cellular toxicity. *Proc. Natl. Acad. Sci.* **105**, 6439–6444.
673 (doi:10.1073/pnas.0802082105)
674 41. Kachroo AH, 1, Laurent JM, Yellman CM, Meyer AG, 1 2, Claus O. Wilke, 1, 2
675 3, Marcotte EM. 2015 Systematic humanization of yeast genes reveals conserved
676 functions and genetic modularity. *Science (80-.).* **348**, 921–925.
677 (doi:10.1126/science.aaa0769)
678 42. William G, Christine S, Bhabatosh C. 1999 Role of mitochondria and C-terminal
679 membrane anchor of Bcl-2 in Bax induced growth arrest and mortality in
680 Saccharomyces cerevisiae . *FEBS Lett.* **380**, 169–175. (doi:10.1016/0014-
681 5793(96)00044-0)
682 43. Xu Q, Reed JC. 2018 Bax Inhibitor-1, a Mammalian Apoptosis Suppressor
683 Identified by Functional Screening in Yeast. *Mol. Cell* **1**, 337–346.
684 (doi:10.1016/S1097-2765(00)80034-9)
685 44. Manon S, Chaudhuri B, Guérin M. 1997 Release of cytochrome c and decrease
686 of cytochrome c oxidase in Bax-expressing yeast cells, and prevention of these
687 effects by coexpression of Bcl-xL. *FEBS Lett.* **415**, 29–32.
688 (doi:https://doi.org/10.1016/S0014-5793(97)01087-9)
689 45. Liang X, Dickman MB, Becker DF. 2014 Proline biosynthesis is required for
690 endoplasmic reticulum stress tolerance in Saccharomyces cerevisiae. *J. Biol.*
691 *Chem.* **289**, 27794–27806. (doi:10.1074/jbc.M114.562827)
692 46. Wuolikainen A, Jonsson P, Ahnlund M, Antti H, Marklund SL, Moritz T,
693 Forsgren L, Andersen PM, Trupp M. 2016 Multi-platform mass spectrometry
694 analysis of the CSF and plasma metabolomes of rigorously matched amyotrophic

695 lateral sclerosis, Parkinson's disease and control subjects. *Mol. BioSyst.* **12**,
696 1287–1298. (doi:10.1039/C5MB00711A)
697 47. Kori M, Aydın B, Unal S, Arga KY, Kazan D. 2016 Metabolic Biomarkers and
698 Neurodegeneration: A Pathway Enrichment Analysis of Alzheimer's Disease,
699 Parkinson's Disease, and Amyotrophic Lateral Sclerosis. *Omi. A J. Integr. Biol.*
700 **20**, 645–661. (doi:10.1089/omi.2016.0106)
701 48. Blasco H *et al.* 2017 Lipidomics Reveals Cerebrospinal-Fluid Signatures of ALS.
702 *Sci. Rep.* **7**. (doi:10.1038/s41598-017-17389-9)
703 49. H. B, F. P, B. MH, H. GP, P. V, R. AC, P. C. 2016 Metabolomics in amyotrophic
704 lateral sclerosis: how far can it take us? *Eur. J. Neurol.* **23**, 447–454.
705 (doi:10.1111/ene.12956)
706 50. Valbuena GN, Rizzardini M, Cimini S, Siskos AP, Bendotti C, Cantoni L, Keun
707 HC. 2016 Metabolomic Analysis Reveals Increased Aerobic Glycolysis and
708 Amino Acid Deficit in a Cellular Model of Amyotrophic Lateral Sclerosis. *Mol.*
709 *Neurobiol.* **53**, 2222–2240. (doi:10.1007/s12035-015-9165-7)
710 51. Dodge JC *et al.* 2015 Glycosphingolipids are modulators of disease pathogenesis
711 in amyotrophic lateral sclerosis. *Proc. Natl. Acad. Sci.*
712 (doi:10.1073/pnas.1508767112)
713 52. Henriques A *et al.* 2015 Amyotrophic lateral sclerosis and denervation alter
714 sphingolipids and up-regulate glucosylceramide synthase. *Hum. Mol. Genet.*
715 (doi:10.1093/hmg/ddv439)
716 53. Alberti S, Gitler AD, Lindquist S. 2007 A suite of Gateway® cloning vectors for
717 high-throughput genetic analysis in Saccharomyces cerevisiae. *Yeast* **24**, 913–
718 919. (doi:10.1002/yea.1502)
719 54. von der Haar T. 2007 Optimized Protein Extraction for Quantitative Proteomics

720 of Yeasts. *PLoS One* **2**, e1078. (doi:10.1371/journal.pone.0001078)

721 55. Chen C, Buhl E, Xu M, Croset V, Rees JS, Lilley KS, Benton R, Hodge JJL,
722 Stanewsky R. 2015 Drosophila Ionotropic Receptor 25a mediates circadian clock
723 resetting by temperature. *Nature* **527**, 516–520. (doi:10.1038/nature16148)

724 56. Mellacheruvu D *et al.* 2013 The CRAPome: a contaminant repository for affinity
725 purification-mass spectrometry data. *Nat. Methods* **10**, 730–6.
726 (doi:10.1038/nmeth.2557)

727 57. Wagih O, Parts L. 2014 gitter: A Robust and Accurate Method for Quantification
728 of Colony Sizes From Plate Images. *G3: Genes|Genomes|Genetics* **4**,
729 547–552. (doi:10.1534/g3.113.009431)

730 58. Wagih O *et al.* 2013 SGAtools: One-stop analysis and visualization of array-
731 based genetic interaction screens. *Nucleic Acids Res.* **41**.
732 (doi:10.1093/nar/gkt400)

733 59. Balakrishnan R, Park J, Karra K, Hitz BC, Binkley G, Hong EL, Sullivan J,
734 Micklem G, Cherry JM. 2012 YeastMine-An integrated data warehouse for
735 Saccharomyces cerevisiae data as a multipurpose tool-kit. *Database* **2012**.
736 (doi:10.1093/database/bar062)

737 60. Shannon P, Markiel A, Ozier O, Baliga NS, Wang JT, Ramage D, Amin N,
738 Schwikowski B, Ideker T. 2003 Cytoscape: a software environment for
739 integrated models of biomolecular interaction networks. *Genome Res.* **13**, 2498–
740 504. (doi:10.1101/gr.1239303)

741 61. Palomino-Schätzlein M, Molina-Navarro MM, Tormos-Pérez M, Rodríguez-
742 Navarro S, Pineda-Lucena A. 2013 Optimised protocols for the metabolic
743 profiling of S. cerevisiae by1H-NMR and HRMAS spectroscopy. *Anal. Bioanal.*
744 *Chem.* **405**, 8431–8441. (doi:10.1007/s00216-013-7271-9)

745 62. Thévenot EA, Roux A, Xu Y, Ezan E, Junot C. 2015 Analysis of the Human
746 Adult Urinary Metabolome Variations with Age, Body Mass Index, and Gender
747 by Implementing a Comprehensive Workflow for Univariate and OPLS
748 Statistical Analyses. *J. Proteome Res.* **14**, 3322–3335.
749 (doi:10.1021/acs.jproteome.5b00354)
750 63. Fahy E, Sud M, Cotter D, Subramaniam S. 2007 LIPID MAPS online tools for
751 lipid research. *Nucleic Acids Res.* (doi:10.1093/nar/gkm324)
752
753
754 **Figure Legends**
755 Figure 1. Expression of OPTN is toxic to yeast. a) Growth in liquid culture showed a
756 reduced maximum exponential growth rate for cells expressing OPTN (red) compared
757 to YFP (black). There was no phenotype for cells expressing OPTN-E478G (blue). b)
758 Fluorescence microscopy showed diffuse cytoplasmic fluorescence for YFP alone,
759 whereas OPTN-YFP formed focal aggregates. There was no observable fluorescence for
760 OPTN-E478G with the same exposure (not shown). c) Spot-tests comparing growth on
761 Glucose (expression off) to Galactose (expression on) showed a growth phenotype for
762 OPTN that was similar to TDP43, and a weaker phenotype for OPTN-E478G.
763
764 Figure 2. Metabolic ES variations observed for yeast overexpressing OPTN versus
765 controls using data from targeted MS data and untargeted NMR profiles. Statistically
766 significant differences ($p<0.05$) are shown as orange and green bars.
767

768 Figure 3. Enriched metabolic pathways observed for yeast overexpressing OPTN versus

769 controls using data from targeted MS data and untargeted NMR profiles in

770 Metaboanalyst 4.0.

771

772

773 **Tables**

774

775

	Reference	SGA screen enhancers (n=58)				
GO biological process term	#	#	expected	Fold Enrichment	+/-	P value
mitochondrion-endoplasmic reticulum membrane tethering	5	3	0.04	69.53	+	2.83E-02
organelle localization by membrane tethering	42	6	0.36	16.55	+	4.19E-03
membrane docking	42	6	0.36	16.55	+	4.19E-03
phospholipid transport	24	5	0.21	24.14	+	5.21E-03
ER to Golgi vesicle-mediated transport	88	7	0.76	9.22	+	2.54E-02
Golgi vesicle transport	195	14	1.68	8.32	+	2.09E-06
vesicle-mediated transport	402	17	3.47	4.9	+	6.77E-05
membrane organization	219	10	1.89	5.29	+	3.85E-02
Unclassified	702	4	6.06	0.66	-	0.00E+00

776

777 Table 1. GO biological process term enrichment for enhancer hits. Enrichment of terms

778 for the 58/64 enhancers that were mapped in the PANTHER database. The +/- column

779 indicates enrichment (+) or depletion (-) of the corresponding term in the enhancers

780 gene set. Enrichment calculated with PANTHER release 20170413 and GO release

781 2017-10-24. P values are shown after applying Bonferroni correction for multiple

782 testing.

783

784

Effect	ALS genes	Deletion systematic name	Deletion standard name	Human ortholog
Enhancer	OPTN, FUS	YHR030C	SLT2	MAPK7
Enhancer	OPTN, FUS	YDR148C	KGD2	DLST
Enhancer	OPTN, FUS	YNL052W	COX5A	COX4I1, COX4I2
Enhancer	TDP43, FUS	YML009C	MRPL39	MRPL33
Suppressor	OPTN, FUS	YBL027W	RPL19B	RPL19
Suppressor	OPTN, FUS	YDR382W	RPP2B	RPLP2

Table 2. Genetic modifiers identified for multiple ALS genes in yeast. OPTN modifiers identified in this paper, TDP43 modifiers from Armakola et al.[35], FUS modifiers from Sun et al.[33].

806

807

808

809

810

811

812

813

Lipid family		Increased	Decreased
FA01	Fatty acids and conjugates	3	2
ST01	Sterols	3	
GL02	Diradylglycerols (DAG)	5	
GL03	Triradylglycerols (TAG)	2	
GP01	Glycerophosphocholines	1	
GP10	Glycerophosphates	1	
SP02	Ceramides	2	
SP05	Neutral glycosphingolipids	1	
Unknown	-	2	

814

815 Table 3. Identified lipid families[63] with differential levels in the LC-MS profiled

816 endometabolome of OPTN yeast vs control.

817

818

819

820

821

822

823

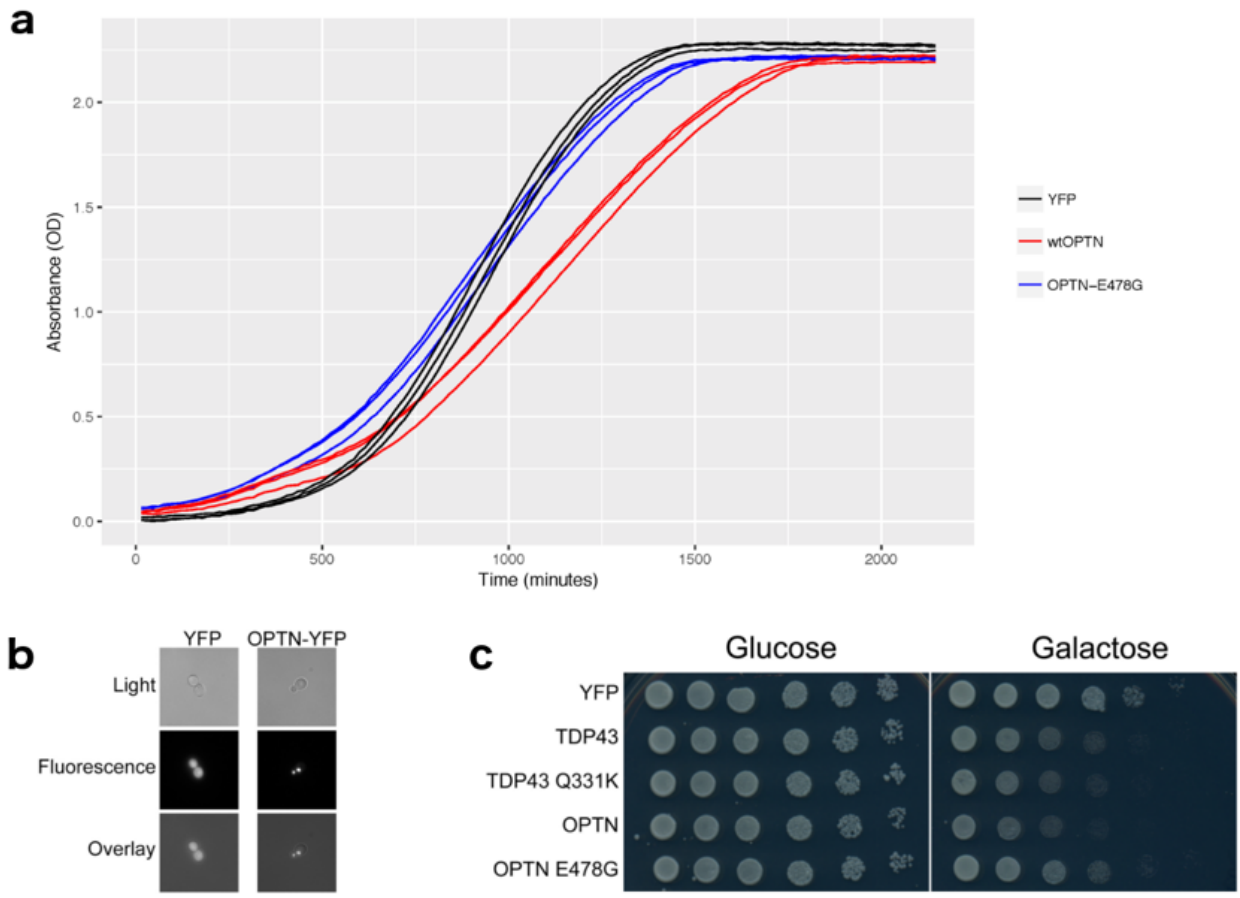

Figure 1. Expression of OPTN is toxic to yeast. a) Growth in liquid culture showed a reduced maximum exponential growth rate for cells expressing OPTN (red) compared to YFP (black). There was no phenotype for cells expressing OPTN-E478G (blue). b) Fluorescence microscopy showed diffuse cytoplasmic fluorescence for YFP alone, whereas OPTN-YFP formed focal aggregates. There was no observable fluorescence for OPTN-E478G with the same exposure (not shown). c) Spot-tests comparing growth on Glucose (expression off) to Galactose (expression on) showed a growth phenotype for OPTN that was similar to TDP43, and a weaker phenotype for OPTN-E478G.

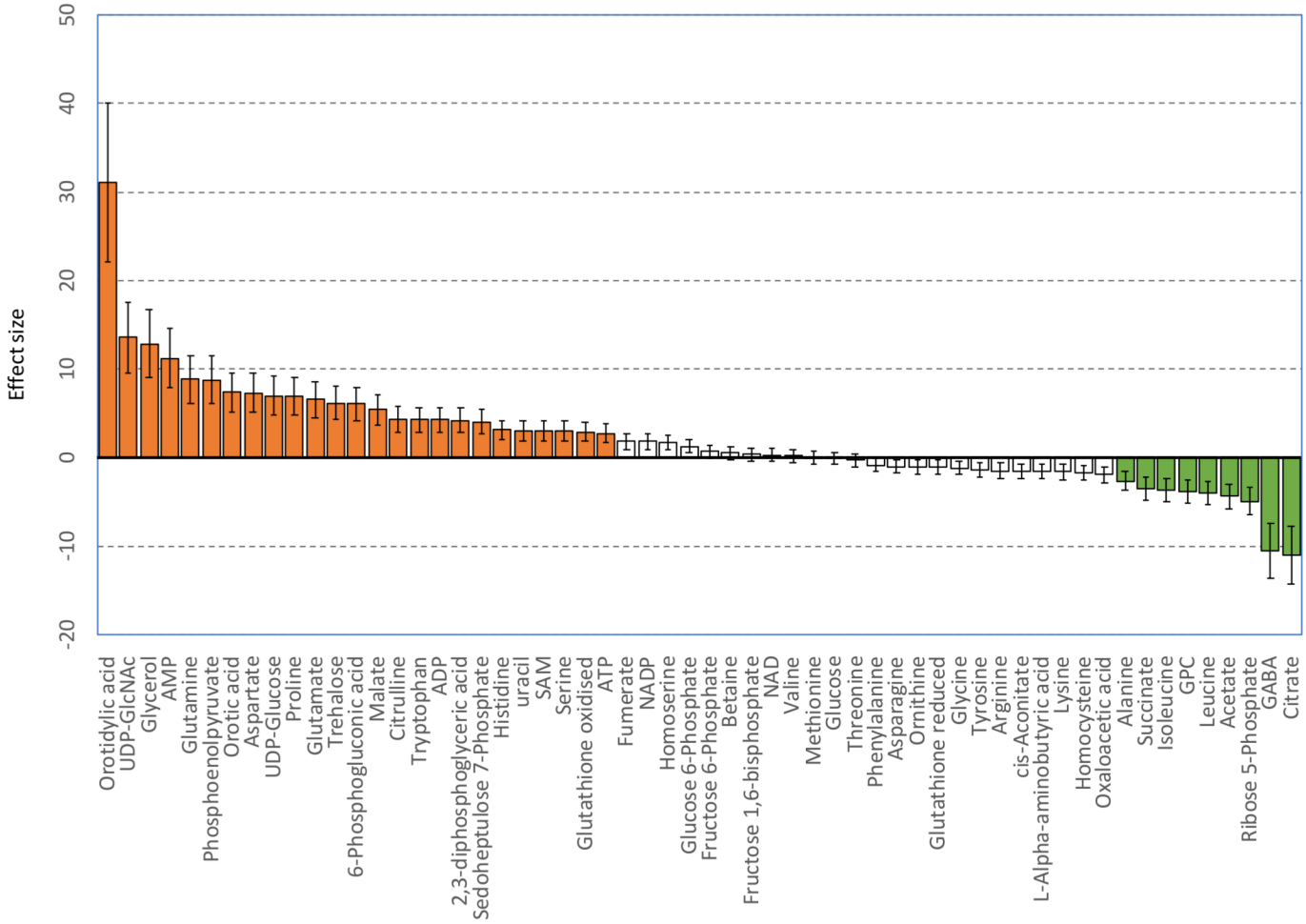

Figure 2. Metabolic ES variations observed for yeast overexpressing OPTN versus controls using data from targeted MS data and untargeted NMR profiles. Statistically significant differences ($p<0.05$) are shown as orange and green bars.

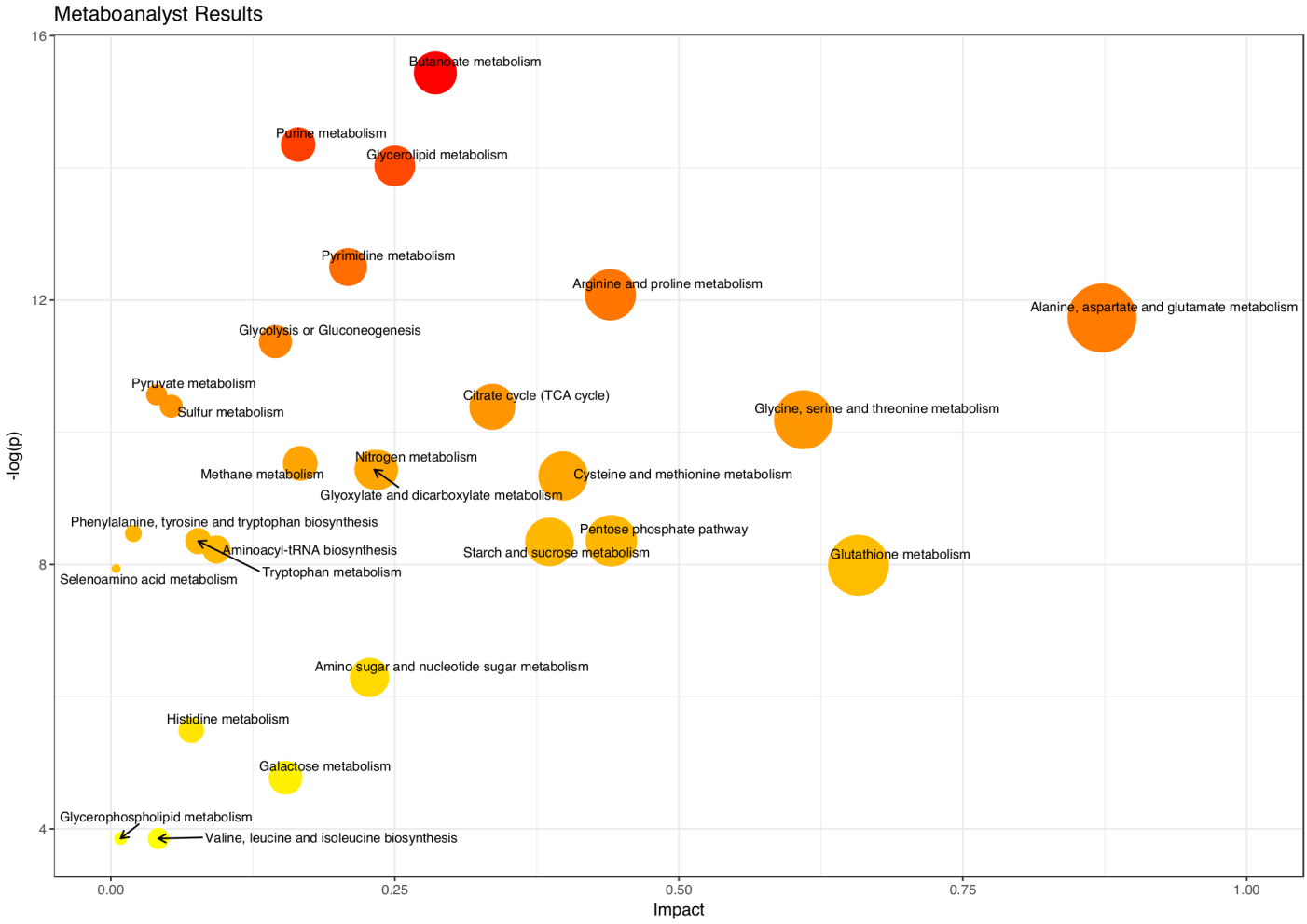

Figure 3. Enriched metabolic pathways observed for yeast overexpressing OPTN versus controls using data from targeted MS data and untargeted NMR profiles in Metaboanalyst 4.0.